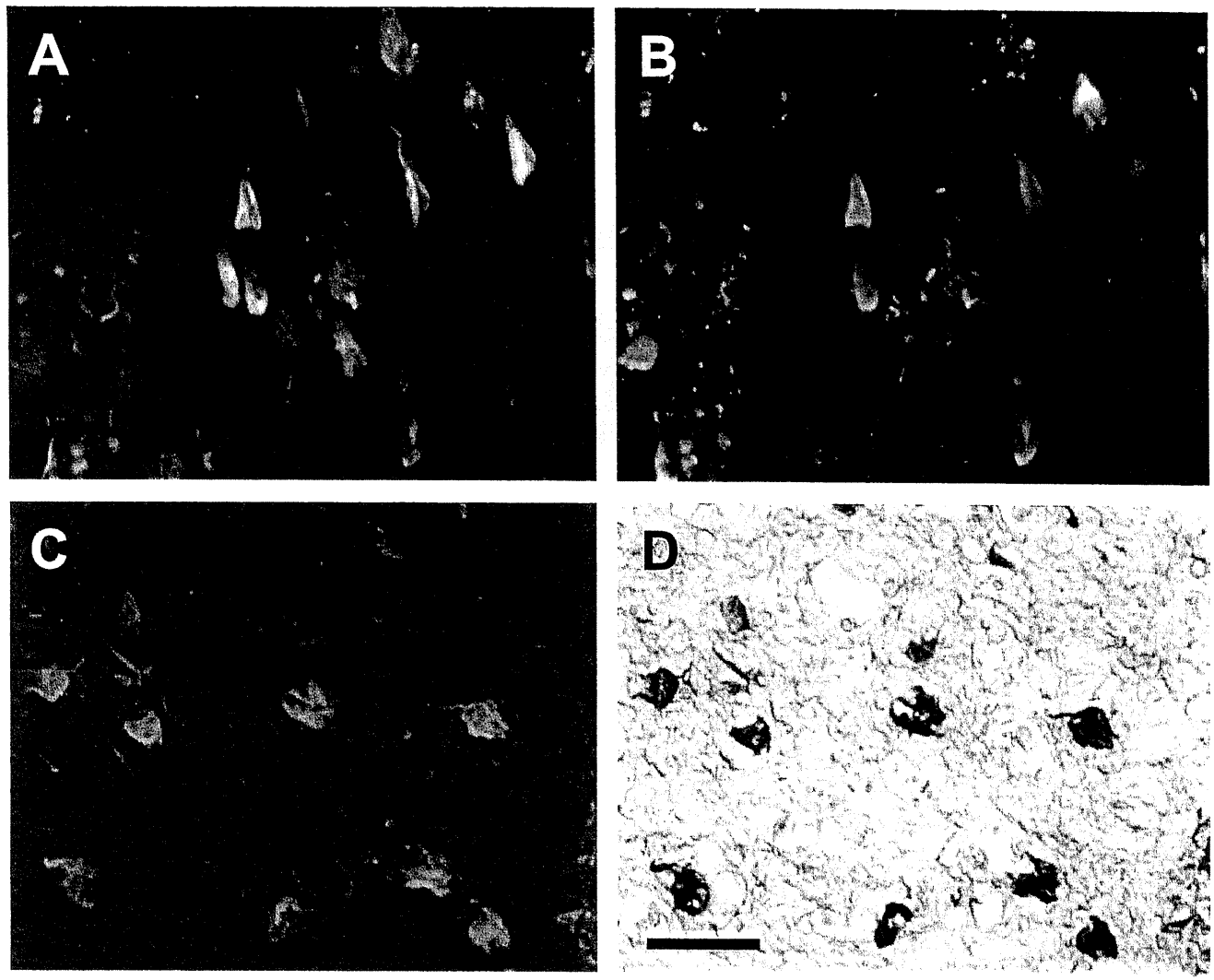
A
B
C
D

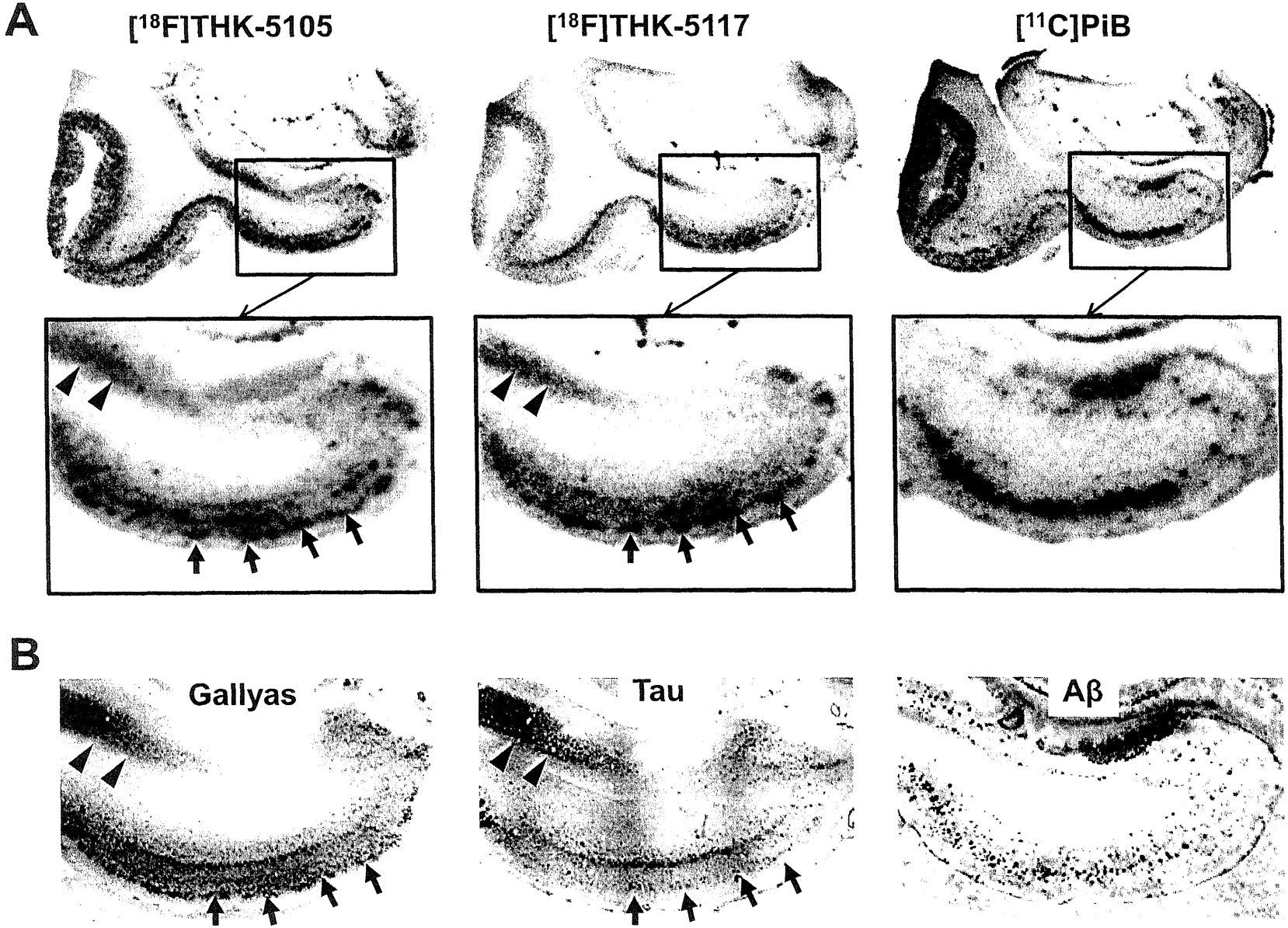
A
[18F]THK-5105
[18F]THK-5117
[11C]PiB
B
Gallyas
Tau
Aβ

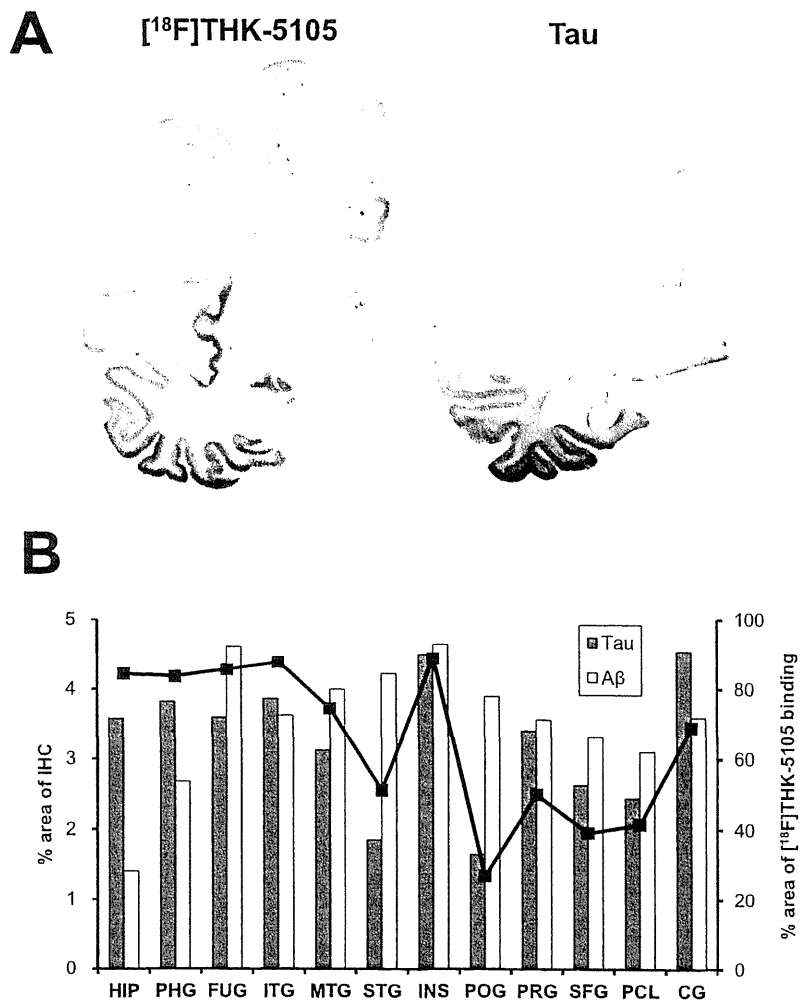
A
[18F]THK-5105
Tau
B
% area of IHC
% area of [18F]THK-5105 binding
Tau
Aβ
HIP
PHG
FUG
ITG
MTG
STG
INS
POG
PRG
SFG
PCL
CG

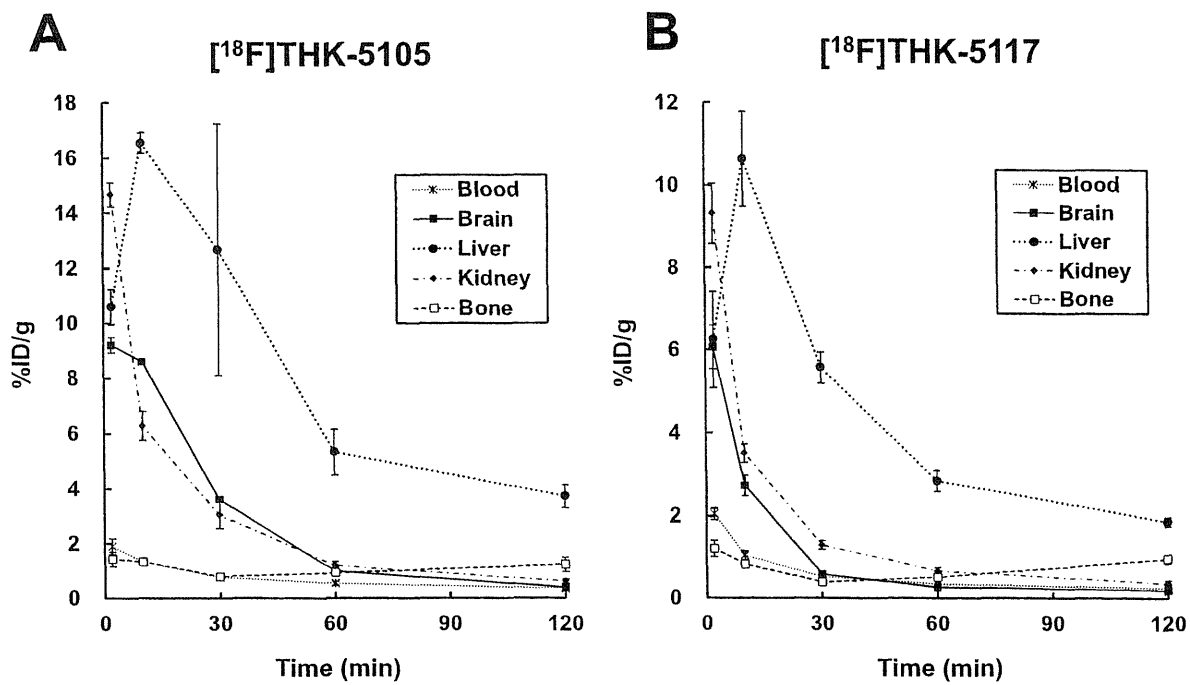
A
[18F]THK-5105
%ID/g
Time (min)
Blood
Brain
Liver
Kidney
Bone
B
[18F]THK-5117
%ID/g
Time (min)
Blood
Brain
Liver
Kidney
Bone

MOLECULAR IMAGING AND BIOLOGY

Mol Imaging Biol (2013)
DOI: 10.1007/s11307-012-0608-5

World Molecular Imaging Society

RESEARCH ARTICLE

A ^{18}F-Labeled BF-227 Derivative as a Potential Radioligand for Imaging Dense Amyloid Plaques by Positron Emission Tomography

Shozo Furumoto,[1,2] Nobuyuki Okamura,[1] Katsutoshi Furukawa,[3] Manabu Tashiro,[4] Yoichi Ishikawa,[2] Kentaro Sugi,[1] Naoki Tomita,[3] Masaaki Waragai,[3] Ryuichi Harada,[1] Tetsuro Tago,[2] Ren Iwata,[2] Kazuhiko Yanai,[1] Hiroyuki Arai,[3] Yukitsuka Kudo[5]

[1]*Department of Pharmacology, Tohoku University School of Medicine, 2-1 Seiryo-machi, Aoba-ku, Sendai 980-8575, Japan*
[2]*Division of Radiopharmaceutical Chemistry, Cyclotron and Radioisotope Center, Tohoku University, Sendai, Japan*
[3]*Department of Geriatrics and Gerontology, Division of Brain Sciences, Institute of Development, Aging and Cancer, Tohoku University, Sendai, Japan*
[4]*Division of Cyclotron Nuclear Medicine, Cyclotron and Radioisotope Center, Tohoku University, Sendai, Japan*
[5]*Clinical Research, Innovation and Education Center, Tohoku University Hospital, Sendai, Japan*

Abstract

Purpose: The aims of this study were to evaluate the binding and pharmacokinetics of novel ^{18}F-labeled ethenyl-benzoxazole derivatives (i.e., [^{18}F] fluorinated amyloid imaging compound of Tohoku university ([^{18}F]FACT)) as amyloid positron emission tomography (PET) tracers and to assess [^{18}F]FACT efficacy in imaging of Alzheimer's disease (AD).

Procedures: Binding assay was conducted using synthetic amyloid-β (Aβ) fibrils, fluorescence microscopy, and autoradiogram in three postmortem AD brains. Pharmacokinetics of [^{18}F]FACT was assessed using 12 Crj:CD-1 (ICR) mice. *In vivo* binding ability with brain amyloid was investigated using amyloid precursor protein (APP) transgenic mouse. Clinical PET scanning using [^{18}F]FACT was performed in ten healthy controls and ten mild cognitive impairment and ten AD patients.

Results: [^{18}F]FACT showed high binding affinity for synthetic Aβ fibrils, preferential binding to dense cored plaques in brain sections, and excellent brain uptake and rapid clearance in mice. Injection in APP mice resulted in specific *in vivo* labeling of amyloid deposits in the brain. PET scans of AD patients showed significantly higher [^{18}F]FACT uptake in the neocortex compared to controls ($P<0.05$, Kruskal–Wallis test).

Conclusion: [^{18}F]FACT is a promising agent for imaging dense Aβ plaques in AD.

Key words: Alzheimer's disease, Amyloid, Early diagnosis, Positron emission tomography

Introduction

Alzheimer's disease (AD) is an age-dependent and irreversible neurodegenerative disorder leading to deterioration of memory and cognitive function. Although the exact mechanisms underlying pathogenesis of AD are not fully understood, formation of brain amyloid plaques through aggregation and deposition of amyloid-β protein (Aβ) is considered to be the initial pathogenic event that may precede the appearance of clinical AD symptoms by decades. Recently, new criteria for diagnosing AD were proposed by the National Institute on Aging—Alzheimer's Association workgroups [1]. The new diagnostic criteria include the use of biomarkers for amyloid deposition to aid

Correspondence to: Nobuyuki Okamura; *e-mail:* nookamura@med.tohoku.ac.jp

Published online: 30 January 2013

in diagnosis of AD. Thus, *in vivo* detection of amyloid depositions with positron emission tomography (PET) has received much attention as a potential technology for early or presymptomatic diagnosis of AD. For this purpose, a number of radiotracers for Aβ aggregates have been synthesized and evaluated as candidates for PET amyloid imaging agents, and some of these are undergoing clinical investigation [2–4].

Among them, *N*-methyl-[^{11}C]-2-(4′-methylaminophenyl)-6-hydroxybenzothiazole ([^{11}C]Pittsburgh compound B, [^{11}C]PiB) is currently the most widely used in clinical research [5]. Labeling of PET tracers with ^{18}F ($T_{1/2}$= 109.8 min) allows time for their delivery to numerous PET centers and contributes to spreading their use. Several ^{18}F-labeled amyloid PET tracers, including [^{18}F]flutemetamol, [^{18}F]florbetaben, [^{18}F]florbetapir, and [^{18}F]AZD4694, have been developed, and to date, [^{18}F]florbetapir has become commercially available [6–9]. An increasing number of PET studies in humans have clearly demonstrated that amyloid PET is a potentially useful technique to visualize and quantify the distribution of Aβ plaques of AD patients [5]. In addition, a proportion of elderly normal subjects present with [^{11}C]PiB retention in the neocortex [10–12], suggesting that amyloid PET is potentially useful for presymptomatic detection of Aβ pathology. Although neocortical PiB retention is considered as a high risk for future cognitive decline, not all PiB-positive normal individuals are destined to develop dementia. Some additional biomarkers are thus necessary for accurate prediction of future conversion to dementia. According to previous histopathological study, progression to dementia is associated with a shift from non-fibrillar to fibrillar amyloid deposits in the brain [13]. Thus, selective detection of dense fibrillar amyloid might be advantageous for predicting progression to dementia.

Previously, we had succeeded in developing a unique scaffold of a radioligand, [^{11}C]2-(2-[2-dimethylaminothiazol-5-yl]ethenyl)-6-(2-[fluoro]ethoxy)benzoxazole ([^{11}C]BF-227), as an amyloid imaging probe [3, 14]. Our previous study demonstrated that Aβ deposits in AD patients can be clearly detected by [^{11}C]BF-227 PET [15]. Neocortical [^{11}C]BF-227 retention was further observed in subjects with mild cognitive impairment (MCI) [16]. Using [^{11}C]BF-227 PET, we achieved a sensitivity of 100 % and a specificity of 71.4 % in distinguishing MCI converters to AD from MCI non-converters [17], suggesting the usefulness of this radiotracer for accurate prediction of future progression to dementia. To further take advantage of this imaging potential, especially in a large clinical study, we anticipated that a ^{18}F-labeled derivative of BF-227 would be valuable due to the longer half-life of ^{18}F compared with ^{11}C.

In this study, we performed a biological evaluation of a series of ^{18}F-labeled 2-ethenyl-benzoxazole derivatives (Fig. 1) to select a candidate for clinical application. The one selected, [^{18}F]Fluorinated Amyloid Imaging Compound of Tohoku University ([^{18}F]FACT), was further evaluated for its binding characteristics with Aβ fibrils and plaques and then for its clinical utility as a probe for imaging amyloid in AD.

Methods

Radiosynthesis of ^{18}F-Labeled 2-Ethenyl-Benzoxazole Derivatives

The chemical structures of the 2-ethenyl-benzoxazole derivatives are summarized in Fig. 1. The compounds and their precursors for ^{18}F-labeling were synthesized according to the method described previously [18]. ^{18}F-labeled compounds were prepared according to the following method. The aqueous $^{18}F^-$ contained in K_2CO_3 solution (1.27 to 3.28 GBq) and Kryptofix 2.2.2 were put into a brown vial, and then the water was azeotropically removed with acetonitrile by heating at 110 °C and He-gas flow. After drying, the activated [^{18}F]KF/Kryptofix 2.2.2. was reacted with a tosylate precursor in dimethyl sulfoxide (DMSO) at 110 °C for 10 min, followed by addition of water to quench. The product was extracted by solid-phase extraction with Sep-Pak ^{t}C18 cartridge (Waters) and then eluted with ethanol. The ^{18}F-labeled compound was separated from the eluent by semi-preparative reversed-phase high-performance liquid chromatography (RP-HPLC), isolated from the collected fraction by solid-phase extraction with Sep-Pak ^{t}C18

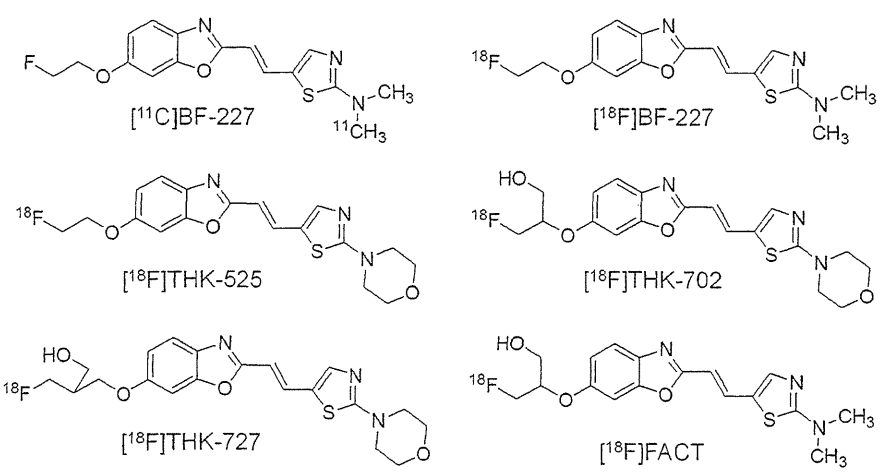

Fig. 1. Chemical structures of [^{11}C]BF-227 and its ^{18}F-labeled 2-ethenyl benzoxazole derivatives.

cartridge, and finally dissolved in DMSO or saline with polysorbate-80 (<0.1 %) for biological evaluation.

[^{11}C]BF-227 was synthesized from the precursor by *N*-methylation with [^{11}C]methyl triflate in DMSO and separated from the crude mixture by semi-preparative RP-HPLC, as described previously [15]. The purified [^{18}F]FACT and [^{11}C]BF-227 were solubilized in isotonic saline containing 1 % polysorbate-80 and 5 % ascorbic acid and then filter-sterilized with 0.22 μm Millipore filter for clinical use.

Fluorescent Staining

Postmortem brain tissue from a 69-year-old man with autopsy-confirmed AD was obtained from Fukushimura Hospital (Toyohashi, Japan). Experiments were performed under the regulations of the hospital ethics committee. Serial sections (6 μm) taken from paraffin-embedded blocks of the temporal cortex were prepared in xylene and ethanol. Before staining with test compounds, quenching of autofluorescence was performed. The quenched tissue section was immersed in 100 μM of test compounds containing 50 % ethanol for 10 min. The stained section was then dipped briefly into water before coverslipping with FluorSave Reagent (Calbiochem, La Jolla, CA, USA) and examination using an Eclipse E800 microscope (Nikon, Tokyo, Japan) equipped with a V-2A filter set (excitation 380 to 420 nm, dichroic mirror 430 nm, long pass filter 450 nm). An adjacent section was immunostained using 4G8 (Signet, Dedham, MA, USA), a monoclonal antibody against Aβ. After pretreatment with 90 % formic acid for 5 min, sections were immersed in blocking solution for 30 min and then incubated for 60 min at 37 °C with 4G8 at a dilution of 1:100. After incubation, sections were processed with biotinylated anti-mouse IgG (Wako) for 60 min, followed by Texas Red-conjugated streptavidin (Vector Laboratories, Burlingame, CA, USA).

In Vitro Autoradiography

A temporal brain section from a 76-year-old female AD patient was incubated with 1.85 MBq/ml of [^{18}F]FACT at room temperature for 20 min and then washed briefly with water and 70 % ethanol. After drying, the labeled section was exposed to a BAS-III imaging plate (Fuji Film, Tokyo, Japan) for 120 min. Autoradiograms were obtained using a BAS-5000 phosphor imaging instrument (Fuji Film, Tokyo, Japan). Neighboring sections were immunostained using 4G8 anti-Aβ monoclonal antibody. After incubation with 4G8, sections were processed by the avidin–biotin method using a Pathostain ABC-POD(M) Kit (Wako, Osaka, Japan) and diaminobenzidine tetrahydrochloride.

In Vitro Binding Study

Amyloid β_{1-40} (Peptide Institute, Inc., Japan) was dissolved in 50 mM potassium phosphate buffer (pH 7.4) to a final concentration of 20 μM. To prepare amyloid fibrils, the solution was incubated at 37 °C for 4 days at 85 rpm and then sonicated to obtain a uniform suspension. The fibril solution was diluted to 2 μM with phosphate-buffered saline (PBS) containing 0.1 % bovine serum albumin (BSA). For saturation binding assay, 100 μl of the fibril solution was mixed with [^{18}F]FACT solution (0.2 to 800 nM, PBS containing 0.1 % BSA and 2 % DMSO, 100 μl) in a 96-well plate. Non-specific binding was defined in the presence of 2 μM FACT in the final solution. The mixture was incubated for 40 min at room temperature and then was passed through the glass filter plate under vacuum with MultiScreen HTS Vacuum Manifold (Millipore Corp., USA), followed by washing with PBS containing 0.1 % BSA twice. Radioactivity of the filter was counted with an automatic gamma counter. The binding data were analyzed with curve-fitting software that calculates the K_d and B_{max} using non-linear regression (GraphPad Prism Version 5.0, GraphPad Software, San Diego, CA, USA).

Biodistribution Study in Normal Mice

The experimental protocols were reviewed by the Committee on the Ethics of Animal Experiments at Tohoku University School of Medicine and performed in accordance with the Guidelines for Animal Experiments issued by the Tohoku University School of Medicine. Male Crj:CD-1 (ICR) mice (6 weeks old, 25 to 30 g, $n=12$) were injected in a lateral tail vein with ^{18}F-labeled test compounds (370 to 740 kBq) contained in isotonic saline (0.2 ml). The mice were sacrificed by cervical dislocation following heart puncture to obtain blood samples at 2, 30, and 60 min postinjection ($n=4$ at each time point). Tissues of interest were excised and weighed, and the radioactivity was counted in an automatic gamma-counter. Radioactivity uptake data are expressed as percent of injected dose per gram of tissue (%ID/g).

Autoradiography of Aβ Deposits in Living Transgenic Mice

An amyloid precursor protein (APP) transgenic (Tg) mouse (female, 31 months old) and a wild-type littermate (female, 31 months old) were injected with [^{18}F]FACT (37 MBq) *via* tail vein. The mice were sacrificed by cervical dislocation at 2 h postinjection, and the brains were rapidly excised and frozen in liquid nitrogen. Frozen sections of 20 μm thick were prepared from the brains for *ex vivo* autoradiography. Autoradiograms were obtained in the same manner described above. The sections used for autoradiography were then subjected to fluorescent staining with thioflavin-S according to the previously described method [19].

Clinical PET Study Using [^{18}F]FACT

Ten patients with amnestic MCI, ten patients with AD, and ten normal age-matched controls participated in the clinical PET study using [^{18}F]FACT. Please refer to Table 1 for characteristics of participants. [^{11}C]BF-227 PET scan was additionally performed in two patients with AD (70-year-old woman (MMSE score 17) and 79-year-old man (MMSE score 20)) and 1 normal control subject (60-year-old man (MMSE score 30)). The average time interval between [^{18}F]FACT and [^{11}C]BF-227 PET scans was 12±6 months. Diagnosis of probable AD was based on criteria from the National Institute of Neurological and Communicative Disorders and Stroke and the Alzheimer's Disease Related Disorders Association [20]. The diagnosis of amnestic MCI was made according to published criteria described previously [21]. The control subjects were

Table 1. Subject and patient demographics in [^{18}F]FACT PET comparisons

	NC	MCI	AD
N	10	10	10
Gender (F/M)	4/6	7/3	7/3
Age (years)	69.8±8.8 (60–89)	74.2±8.8 (57–89)	74.5±4.6 (66–81)
MMSE score	29.9±0.3 (29–30)	26.4±1.1 (24–28)	19.8±3.0 (15–24)

recruited from volunteers who were taking no centrally acting medications, had no cognitive impairment, and had no cerebrovascular lesions, including asymptomatic cerebral infarction on T2-weighted studies, identified *via* MRI. All volunteers were screened using a questionnaire and medical history, and those with medical conditions potentially affecting the central nervous system were excluded. The Committee on Clinical Investigation at Tohoku University School of Medicine and the Advisory Committee on Radioactive Substances at Tohoku University approved the study protocol. After complete description of the study to the patients and subjects, written informed consent was obtained.

Image Acquisition Protocols

[^{18}F]FACT-PET and [^{11}C]BF-227-PET study was performed using a SET-2400W PET scanner (Shimadzu, Kyoto, Japan). After intravenous injection of 111–185 MBq of [^{18}F]FACT or 211–366 MBq of [^{11}C]BF-227, dynamic PET images were obtained for 60 min (23 sequential scans; 5 scans×30 s, 5 scans×60 s, 5 scans×150 s, and 8 scans×300 s) with the subject's eyes closed. SUV summation images at 0–10, 10–20, 20–30, 30–40, 40–50, and 50–60 min postinjection were created for the analysis of tracer uptake. T1-weighted MR images were obtained using a SIGNA 1.5 T machine (General Electric, Milwaukee, WI, USA).

Image Analysis

Firstly, standardized uptake value (SUV) images of [^{18}F]FACT and [^{11}C]BF-227 were obtained by normalizing tissue radioactivity concentration by injected dose and body weight. Subsequently, individual MR images were anatomically coregistered into individual PET images using Statistical Parametric Mapping software (SPM5: Welcome Department, UK). Regions of interest (ROIs) were placed on individual axial MR images in the cerebellar hemisphere, frontal cortex [Brodmann's areas (BA) 8, 9, 10, 44, 45, 46, and 47], lateral temporal cortex (BA 21, 22, 37, and 38), parietal cortex (BA 39 and 40), occipital cortex (BA 17), anterior cingulate cortex, posterior cingulate cortex, medial temporal cortex (BA 27, 28, 34, and 35), striatum, pons, and subcortical white matter, as described previously [15]. The ROI information was then copied onto dynamic PET SUV images, and regional SUVs were sampled using PMOD software (PMOD Technologies, Ltd., Zurich, Switzerland). The ratio of regional SUV to cerebellar SUV (SUVR) was calculated as an index of tracer retention. Averaged SUVR in the frontal, temporal, parietal, and posterior cingulate cortices was considered representative of tracer retention in the neocortex (neocortical SUVR). The inter-rater reliability for the ROI measurement was tested between two raters (N.O. and K.S.) in seven subjects and patients. The intra-class correlation coefficient was 0.95.

Statistical Analysis

For statistical comparison in the three groups, we applied the Kruskal–Wallis test followed by Dunn's multiple comparison test. Differences of time activity curves (TACs) in [^{18}F]FACT PET were also evaluated by repeated measures ANOVA followed by the Bonferroni–Dunn post hoc test. For statistical comparisons of PET measurements in control and AD groups, we used the Mann–Whitney *U* test. Effect size coefficients (Cohen's *d*) were also calculated for the evaluation of group differences in PET measurements. Statistical significance for each analysis was defined as $P<0.05$. Correlations between [^{18}F]FACT and [^{11}C]BF-227 SUVR in the frontal, temporal, parietal, and occipital cortices of three subjects (two AD and one normal control) were determined using Pearson's correlations. A linear model was applied to the data to obtain a correlation coefficient and *p* value. These analyses were performed using GraphPad Prism5 software (GraphPad, San Diego, CA, USA).

Results

Radiosynthesis

^{18}F-labeled 2-ethenyl-benzoxazole derivatives (Fig. 1) were obtained in yields of 32 % on average (21 to 44 %, decay-corrected) with radiochemical purity greater than 99 % after HPLC purification. The specific activities ranged 70 to 180 GBq/μmol, corrected at the end of synthesis.

In Vitro Binding to Aβ Plaques in AD Brain Sections

Binding ability of 2-ethenyl-benzoxazole derivatives to Aβ plaques was examined using AD brain sections from a 69-year-old man with autopsy-confirmed AD. As shown in Fig. 2a, c, dense cored plaques (arrowheads) were clearly stained with FACT. In particular, Aβ plaque cores were brightly stained with this compound. The fluorescent staining pattern of FACT correlated well with Aβ immunostaining (Fig. 2b) and thioflavin-S staining (Fig. 2d) in adjacent sections. Other compounds produced similar results in the histopathological staining of AD brain sections from a 69-year-old man with autopsy-confirmed AD.

In vitro autoradiography at tracer dose indicated [^{18}F]FACT binding to dense Aβ deposits (arrowheads) in AD temporal brain sections from a 76-year-old female AD patient (Fig. 2e–h). Tracer signals were additionally detected

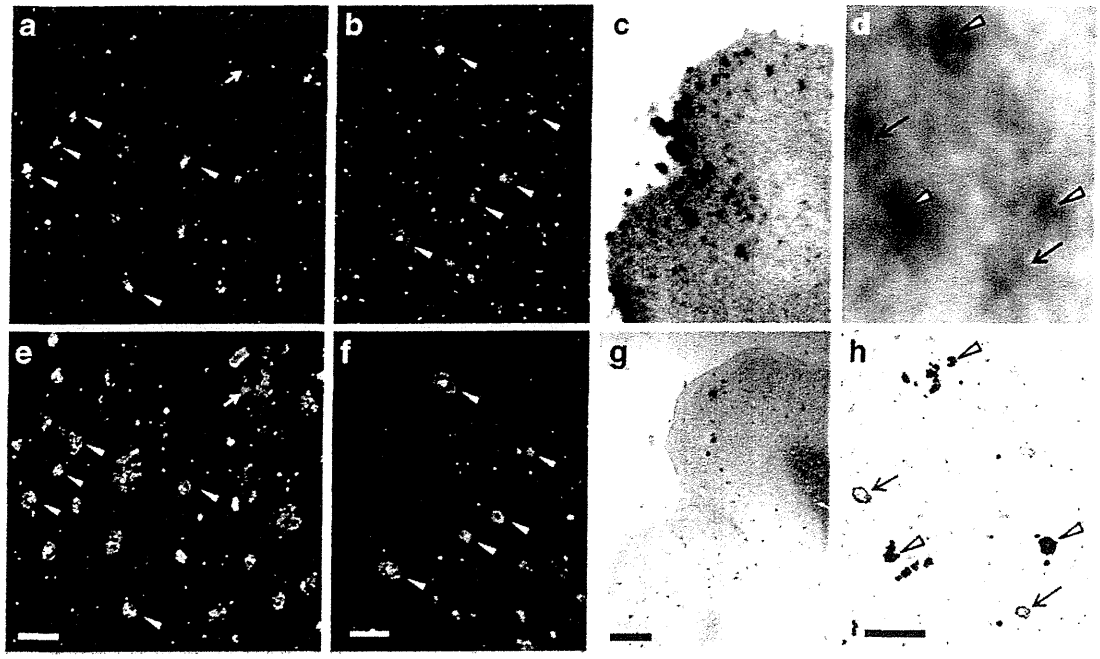

Fig. 2. **a–d** *Fluorescence microscopy images of AD brain sections from a 69-year-old man with autopsy-confirmed AD stained with FACT (**a**, **c**), anti-Aβ (4 G8) antibody (**b**), and thioflavin-S (**d**). Arrowheads delineate dense cored plaques, respectively.* **e–h** *Autoradiogram of AD brain section from a 76-year-old female AD patient with [^{18}F]FACT (**e**, **g**) and images of the adjacent section immunostained with anti-Aβ (4 G8) antibody (**f**, **h**). Arrows and arrowheads delineate congophilic amyloid angiopathy and dense cored plaques, respectively. Bars 100 μm (**a–d**), 2 mm (**e–f**), 200 μm (**g–h**).*

in congophilic amyloid angiopathy (arrows). These results indicated that FACT and its derivatives had an ability to detect pathological dense Aβ deposits in AD brain tissue.

Binding Affinity to Synthetic Aβ Fibrils

Binding properties of [^{18}F]FACT with Aβ fibrils were investigated by *in vitro* binding assay. Scatchard analysis of FACT binding to Aβ fibrils showed two classes of binding sites: a high-affinity site (K_d=9.4 nM; B_{max}= 0.16 pmol/nmol of Aβ) and a low-affinity site (K_d= 263 nM; B_{max}=1.52 pmol/nmol of Aβ).

Biodistribution Study in Normal Mice

Two important properties of an amyloid imaging probe are rapid brain uptake and rapid clearance from the normal brain without non-specific binding. These properties of the ^{18}F-labeled 2-ethenyl-benzoxazole derivatives were evaluated by biodistribution studies in 12 normal mice (n=4 at each time point). The radioactivity uptake in the blood, brain, liver, kidney, and bone is summarized in Table 2. Regarding brain uptake, all of the ^{18}F-labeled derivatives showed rapid and sufficient brain uptake (4 to 6 %ID/g at 2 min) and smooth washout after that. However, the brain uptake at 60 min varied from 0.28 to 1.68 %ID/g, suggesting a different clearance property in normal brain. Among the derivatives, [^{18}F]FACT indicated the highest ratio of brain uptakes at 2 min to that at 60 min (4.64/0.28=16.6). Additionally, mice injected with [^{18}F]FACT exhibited no increase of the radioactivity uptake in bone with time, unlike with [^{18}F]BF-227, suggesting that [^{18}F] FACT has good stability in regard to metabolic defluorination *in vivo*. Thus, we selected [^{18}F]FACT as the candidate for the clinical comparisons.

Autoradiography of Aβ Deposits in Living Transgenic Mouse

In vivo binding ability of [^{18}F]FACT with amyloid plaques was evaluated in the APP-Tg mouse. Autoradiographic images of the APP-Tg mouse brain post-intravenous injection of [^{18}F]FACT displayed high uptake of the labeling compound in the cortex and hippocampus (Fig. 3a). In contrast, no notable binding was observed in the brain of wild-type mouse (Fig. 3b). These [^{18}F]FACT binding results in APP-Tg mouse brain corresponded closely with those of *in vitro* thioflavin-S staining in the same brain sections (Fig. 3c, d). These results warranted further clinical investigation of [^{18}F]FACT PET in AD patients.

Clinical PET Study Using [^{18}F]FACT

Demographic data for the participants are summarized in Table 1. No statistical difference in age was observed among the three groups. MCI and AD patients had significantly lower mean MMSE scores than normal controls (P<0.05,

Table 2. Biodistribution of ^{18}F-labeled compounds in mice

Tracers	Time (min)	Radioactivity uptakes (%ID/g)				
		Blood	Brain	Liver	Kidney	Bone
[^{18}F]BF-227	2	2.93±0.08	6.05±0.45	7.97±1.59	9.63±0.89	1.59±0.27
	30	2.14±0.17	1.91±0.05	5.75±0.42	3.04±0.15	4.38±1.24
	60	2.09±0.15	1.67±0.14	5.48±0.23	2.42±0.20	7.04±0.75
[^{18}F]THK-525	2	2.82±0.38	4.73±1.32	5.93±1.40	7.72±2.44	1.77±0.87
	30	2.20±0.24	2.05±0.16	3.55±0.60	2.32±0.18	6.74±2.20
	60	1.91±0.29	1.68±0.15	2.47±0.23	1.48±0.14	9.65±0.89
[^{18}F]THK-702	2	3.34±0.13	4.15±0.28	7.53±0.50	13.6±0.88	1.95±0.34
	30	1.06±0.19	0.53±0.03	4.55±0.39	1.58±0.64	0.92±0.11
	60	0.67±0.08	0.35±0.04	3.65±0.72	0.65±0.09	1.16±0.70
[^{18}F]THK-727	2	2.94±0.33	4.06±0.26	9.89±4.16	11.4±1.35	2.08±0.39
	30	1.52±0.10	1.04±0.08	6.68±1.22	2.47±0.36	6.61±0.79
	60	0.66±0.10	0.69±0.02	4.04±1.87	0.98±0.14	9.33±1.34
[^{18}F]FACT	2	3.65±0.66	4.64±0.55	9.38±0.43	10.2±1.05	1.84±0.18
	30	1.19±0.49	0.53±0.11	11.3±1.32	4.17±0.44	0.88±0.07
	60	0.64±0.13	0.28±0.04	14.1±0.55	3.25±0.27	1.38±0.46

Data are expressed as mean±SD (n=4 at each time point)

Kruskal–Wallis test). AD patients additionally had significantly lower mean MMSE scores than those with MCI ($P<0.05$, Kruskal–Wallis test). No toxic events were observed in the current clinical trial. The SUV-TACs from [^{18}F]FACT-PET in AD patients and normal control subjects are shown in Fig. 4. Both groups showed rapid entry of [^{18}F]FACT into the neocortex and cerebellum. In the AD patients, the temporal cortex, known to contain high concentrations of fibrillar amyloid plaques in AD, showed retention of [^{18}F]FACT during the later time points compared with the cerebellum (Fig. 4a). In contrast, TACs in the temporal cortex and the cerebellum were nearly identical in normal subjects (Fig. 4b). The subcortical white matter regions showed relatively lower entry and slower clearance than gray matter areas, but no difference in TACs between AD patients and normal controls.

SUVR in the lateral temporal cortex of AD patients was significantly higher over 10 min postinjection of [^{18}F]FACT than those of normal controls ($p<0.05$, Mann–Whitney U test) and reached maximum value at 30 to 40 min postinjection (Fig. 4c). Effect size between AD and normal controls showed the highest value at 30 to 40 min postinjection of [^{18}F]FACT (Table 3). The ratio of SUVR in AD to SUVR in normal controls became constant after

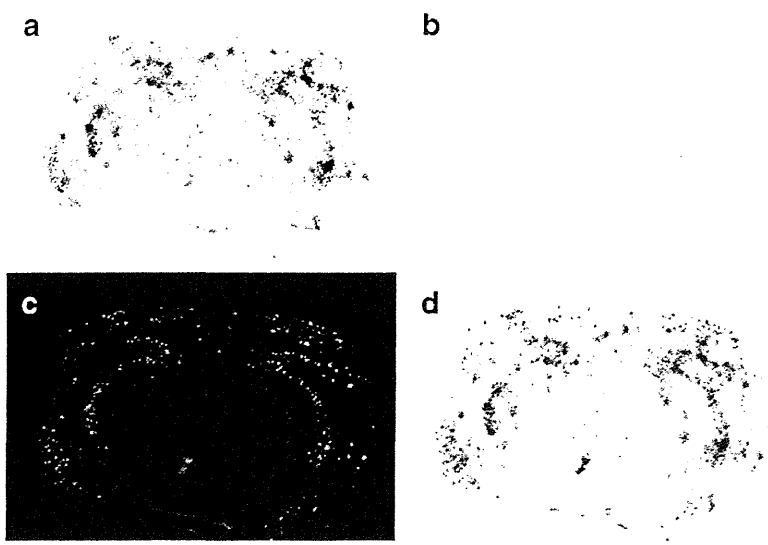

Fig. 3. *Ex vivo* autoradiograms of brain sections from APP transgenic (Tg) mouse (**a**) and wild type mouse (**b**). The brains were excised at 2 h after intravenous injection of [^{18}F]FACT. Aβ plaques in APP-Tg mouse brain were clearly stained with thioflavin-S (**c**). A merged image of **a** and **c** is shown in **d**.

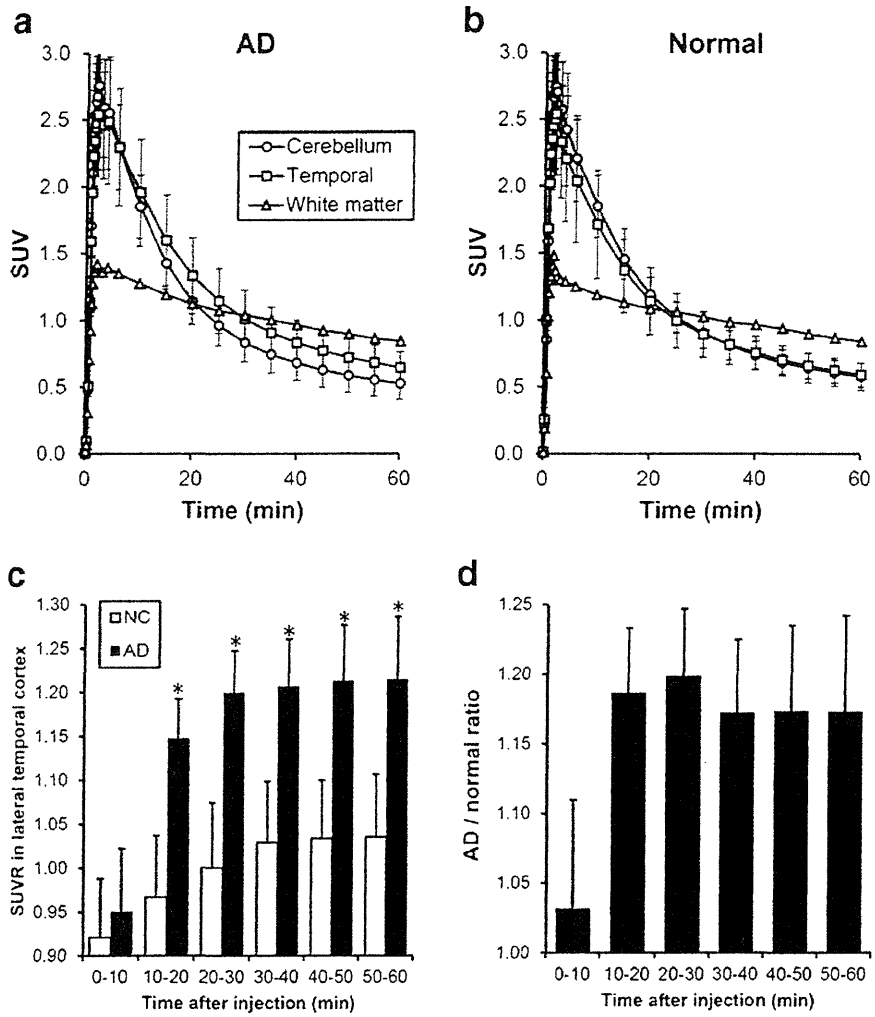

Fig. 4. Time activity data for [^{18}F]FACT PET in humans. Time activity curves of [^{18}F]FACT in ten AD patients (**a**) and ten normal controls (**b**) are shown. Each point represents the mean±standard deviations of data. Time course of [^{18}F]FACT SUVR in the lateral temporal cortex (**c**) and AD *vs* normal ratio of SUVR in the lateral temporal cortex (**d**) are also shown. *P<0.05 by the Mann–Whitney U test.

30 min (Fig. 4d). Based on these results, we selected summed dynamic images from 30 to 40 min for the ROI analysis of PET data.

SUVR images of [^{18}F]FACT for a normal control subject (a 60-year-old man, MMSE score 30) and an AD patient (70-year-old woman, MMSE score 17) are shown in Fig. 5a. Cortical retention of [^{18}F]FACT at 30 to 40 min postinjection was evident in the AD patient, as contrasted with the images of the normal control subject. This pattern of distribution was consistent with the distribution of [^{11}C]BF-227 at 30 to 40 min postinjection in the same subject and patient pair (Fig. 5a). The SUV-TACs from [^{18}F]FACT-PET were compared with those from [^{11}C]BF227-PET in the same AD patient (70-year-old woman, MMSE score 17). As shown in Fig. 5b, [^{18}F]FACT showed faster washout from both temporal cortex and cerebellum than [^{11}C]BF-227. The regional SUVR of [^{18}F]FACT at 30 to 40 min postinjection was compared with that of [^{11}C]BF-227 at the same time frame. SUVR values in the frontal, temporal, parietal, and occipital cortices of three subjects (two AD and one normal control) were used for this analysis. As shown in Fig. 5c, regional SUVR of [^{18}F]FACT were significantly correlated with that of [^{11}C]BF-227 (Pearson's r= 0.931, P<0.001) in these three subjects.

In the quantitative comparison of regional SUVR 30 to 40 min post-administration, the values for the frontal, lateral

Table 3. Time course of lateral temporal [^{18}F]FACT SUVR and effect size measures in ten normal controls and ten AD patients

Time (min)	Normal control	AD	Cohen's d
30–40	1.07±0.06	1.22±0.05*	2.67
40–50	1.08±0.06	1.23±0.06*	2.37
50–60	1.09±0.06	1.23±0.06*	2.34

*P<0.05 by the Mann–Whitney U test

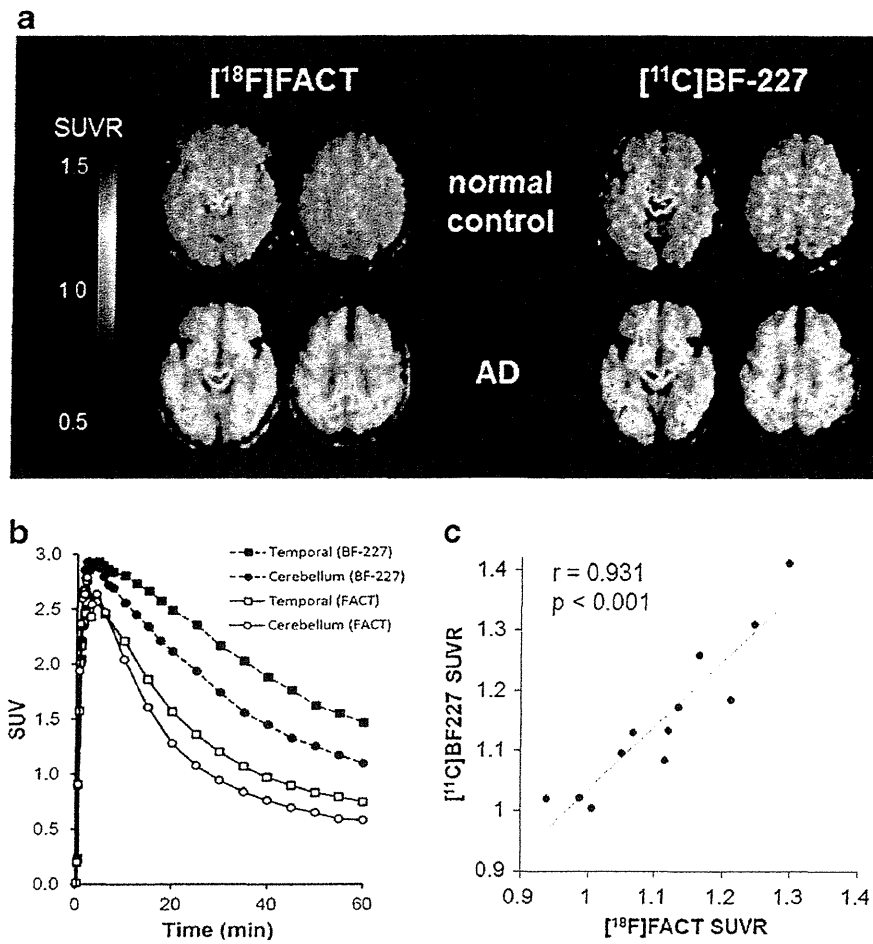

Fig. 5. **a** SUVR images (30 to 40 min postinjection) of [^{18}F]FACT and [^{11}C]BF-227 for a normal control subject (60-year-old man, MMSE score 30) and an AD patient (70-year-old woman, MMSE score 17). **b** Time activity curves of [^{18}F]FACT and [^{11}C]BF-227 in an AD patient (70-year-old woman, MMSE score 17). **c** Significant correlation between regional SUVR of [^{18}F]FACT and [^{11}C]BF-227 in two AD (70-year-old woman (MMSE score 17) and 79-year-old man (MMSE score 20)) and one normal control (60-year-old man, MMSE score 30) subjects (Pearson's r=0.931, P<0.001).

temporal, parietal, occipital, and anterior and posterior cingulate cortices were significantly greater in AD patients than in the normal controls (Table 4). In addition, the SUVRs for the lateral temporal, parietal, occipital, and anterior and posterior cingulate cortices were significantly greater in AD patients than in those with MCI. As shown in Fig. 6, averaged neocortical SUVR was also significantly greater in AD patients than in normal control subjects and MCI (P<0.05, Kruskal–Wallis test). MCI patients additionally showed significantly greater SUVR in the lateral temporal and frontal cortices than normal subjects, but not significant in other brain regions (P<0.05, Kruskal–Wallis

Table 4. Regional SUVR (30 to 40 min postinjection) and effect size measures of [^{18}F]FACT in ten normal controls and ten MCI and ten AD patients

	Normal control	MCI	AD	Cohen's d NC *vs.* AD
Frontal	1.00±0.10	1.09±0.04*	1.15±0.06*	1.82
Lateral temporal	1.05±0.08	1.13±0.06*	1.21±0.05*,**	2.40
Parietal	1.07±0.07	1.13±0.07	1.21±0.08*,**	1.86
Occipital	1.09±0.08	1.07±0.06	1.17±0.05*,**	1.20
Anterior cingulate	1.08±0.07	1.12±0.08	1.21±0.08*,**	1.73
Posterior cingulate	1.15±0.07	1.17±0.06	1.30±0.07*,**	2.14
Medial temporal	1.10±0.05	1.13±0.04	1.15±0.09	0.69
Striatum	1.31±0.11	1.30±0.06	1.35±0.12	0.35
Pons	1.55±0.15	1.57±0.10	1.54±0.09	0.08
White matter	1.50±0.21	1.47±0.11	1.52±0.13	0.12
Neocortex	1.04±0.07	1.12±0.05	1.19±0.05*,**	2.47

*P<0.05 (vs normal control group) and **P<0.05 (vs MCI group) by the Kruskal–Wallis test followed by Dunn's multiple comparison test

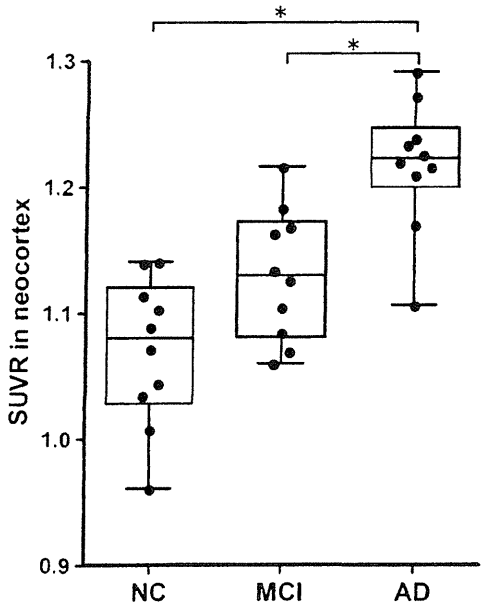

Fig. 6. Comparison of neocortical SUVR of [^{18}F]FACT among ten aged normal controls (NC) and ten mild cognitive impairment (MCI) and ten AD patients. The neocortical SUVRs are represented in a *box* and *whisker plot*. *P<0.05 by the Kruskal–Wallis test followed by Dunn's multiple comparison test.

test). The SUVR in the medial temporal cortex and striatum showed the tendency to be greater in AD patients, but this was not significant. The SUVR in the pons and white matter was nearly identical in AD, MCI, and normal subjects. Effect size value between AD and aged normal subjects was the highest in the lateral temporal cortex (2.40), followed by the posterior cingulate (2.14), parietal (1.86), frontal (1.82), and anterior cingulate (1.73) and occipital (1.20) cortices (Table 4).

Discussion

The current study demonstrated that [^{18}F]FACT PET can be used to detect AD pathology in AD patients and to confirm its absence in cognitively unimpaired elderly people. We previously reported the ability of [^{11}C]BF-227-PET to detect Aβ deposits in the brains of AD patients [15]. The current study has further demonstrated the binding preference of [^{18}F]FACT to dense Aβ plaques in the brains of AD patients. A similar pattern of tracer distribution was observed between [^{18}F]FACT and [^{11}C]BF-227 in AD patients, indicating that [^{18}F]FACT-PET could be substituted for [^{11}C]BF-227-PET for noninvasive detection of dense Aβ deposits in the brain of AD patients. The correlation of [^{18}F]FACT uptake *in vivo* and brain pathology at autopsy should be examined in the future. Our previous studies demonstrated the unique ability of [^{11}C]BF-227 to detect certain forms of prion and α-synuclein protein deposits [22, 23]. Further study will be required to validate the practical usefulness of [^{18}F]FACT-PET for noninvasive detection of these protein deposits.

When a neocortical [^{18}F]FACT SUVR of 1.145 (1.5 SD above control mean) was used as a cutoff, [^{18}F]FACT-PET scan achieved a sensitivity of 90 % (nine of ten) and a specificity of 100 % (ten of ten) in the discrimination between AD patients and normal subjects. In one exception, a 76-year-old female AD patient, MMSE score 24, showed no remarkable retention of [^{18}F]FACT in the neocortex. This is not surprising because approximately 10 to 20 % of patients diagnosed as probable AD reportedly fail to meet pathological criteria for AD at autopsy.

The amnestic subtype of MCI has a high risk of progression to dementia, and it may constitute a prodromal stage of AD [24]. Previous amyloid-PET studies demonstrated a substantial amount of neocortical tracer retention in 50 to 60 % of the MCI population, which is comparable to the level in AD patients [10, 17]. In our study, about half of the MCI patients had elevated neocortical [^{18}F]FACT retention, which was an intermediate level between the aged normal subjects and the AD patients. This finding is in accord with the previous neuropathological observation that the density of neuritic plaque increased as a function of increasing dementia severity [25]. The parent tracer [^{11}C]BF-227 showed neocortical retention to be a reliable indicator of disease progression in MCI subjects in our previous study [17, 19]. Therefore, PET imaging with [^{18}F]FACT is also expected to have a similar prognostic utility.

The amount of elevation of neocortical [^{18}F]FACT uptake in AD patients was approximately 14 to 15 %, far less than PiB and other ^{18}F-labeled amyloid-PET tracers. This is probably due to the relatively low binding affinity and B_{max} of this tracer with amyloid fibrils in comparison to that of PiB (K_d=1.02 nM, B_{max}=0.61) [26, 27]. There is considerable amount of tracer retention in the white matter, which reflects non-specific binding of the compound to myelin sheath. Because of modest specific binding of [^{18}F]FACT in the gray matter of AD patients, spillover from the white matter could reduce the sensitivity for detecting amyloid positive subjects. Use of early phase (30 to 40 min postinjection) images can compensate for this because the relatively stronger signals in the gray matter persist in this time interval. Partial volume correction may also be able to improve the discriminatory power of [^{18}F]FACT-PET by eliminating nonspecific signals in the white matter. Another method to improve the sensitivity for detecting specific signals in the brain is to create a statistical map by comparison with a normal control database [19].

One of advantages of [^{18}F]FACT over BF-227 is its rapid kinetic profile. [^{18}F]FACT showed faster washout from normal brain tissue than BF-227 (Fig. 5) probably because of the lower lipophilicity of FACT (LogP=1.99±0.02) as compared to BF-227 (LogP=2.29±0.02). The neocortical SUVR of [^{18}F]FACT reached a peak at 30 min post-administration. This characteristic would also contribute to reduced procedure and waiting times for PET scans.

Conclusion

We successfully developed a novel ^{18}F-labeled ethenylbenzoxazole derivative, [^{18}F]FACT, as a PET tracer for amyloid deposits. This tracer preferentially bound to dense Aβ plaques in AD brain sections, visualized cortical amyloid deposits in APP Tg mice, and demonstrated fast kinetics and significant retention of [^{18}F]FACT in sites with predilection for the deposition of dense amyloid plaques in AD patients during clinical PET imaging. [^{18}F]FACT PET distinctly distinguished AD patients from normal individuals. These findings suggest that [^{18}F]FACT may be usable for *in vivo* detection of dense Aβ plaques in AD brains.

Acknowledgments. This study was financially supported by the Special Coordination Funds for Promoting Science and Technology, the Health and Labour Sciences Research Grants for Translational research from Ministry of Health, Labour and Welfare, the Program for Promotion of Fundamental Studies in Health Science of the National Institute of Biomedical Innovation, and the Grant-in-Aid for Scientific Research (C) (20591432) from the Ministry of Education, Culture, Sports, Science and Technology of Japan. The authors appreciate the technical assistance of Dr. Shoichi Watanuki in the clinical PET studies.

Conflict of Interest. The authors declare they have no conflicts of interest.

References

1. McKhann GM, Knopman DS, Chertkow H et al (2011) The diagnosis of dementia due to Alzheimer's disease: recommendations from the National Institute on Aging—Alzheimer's Association workgroups on diagnostic guidelines for Alzheimer's disease. Alzheimers Dement 7:263–269
2. Kadir A, Nordberg A (2010) Target-specific PET probes for neurodegenerative disorders related to dementia. J Nucl Med Off Publ Soc Nucl Med 51:1418–1430
3. Furumoto S, Okamura N, Iwata R, Yanai K, Arai H, Kudo Y (2007) Recent advances in the development of amyloid imaging agents. Curr Top Med Chem 7:1773–1789
4. Okamura N, Fodero-Tavoletti MT, Kudo Y et al (2009) Advances in molecular imaging for the diagnosis of dementia. Expert Opin Med Diagn 3:705–716
5. Klunk WE, Engler H, Nordberg A et al (2004) Imaging brain amyloid in Alzheimer's disease with Pittsburgh Compound-B. Ann Neurol 55:306–319
6. Vandenberghe R, Van Laere K, Ivanoiu A et al (2010) ^{18}F-flutemetamol amyloid imaging in Alzheimer disease and mild cognitive impairment: a phase 2 trial. Ann Neurol 68:319–329
7. Barthel H, Gertz HJ, Dresel S et al (2011) Cerebral amyloid-beta PET with florbetaben (^{18}F) in patients with Alzheimer's disease and healthy controls: a multicentre phase 2 diagnostic study. Lancet Neurol 10:424–435
8. Clark CM, Schneider JA, Bedell BJ et al (2011) Use of florbetapir-PET for imaging beta-amyloid pathology. Jama 305:275–283
9. Jureus A, Swahn BM, Sandell J et al (2010) Characterization of AZD4694, a novel fluorinated Abeta plaque neuroimaging PET radioligand. J Neurochem 114:784–794
10. Rowe CC, Ng S, Ackermann U et al (2007) Imaging beta-amyloid burden in aging and dementia. Neurology 68:1718–1725
11. Hatashita S, Yamasaki H (2010) Clinically different stages of Alzheimer's disease associated by amyloid deposition with [^{11}C]-PIB PET imaging. J Alzheimer's Dis JAD 21:995–1003
12. Villemagne VL, Pike KE, Chetelat G et al (2011) Longitudinal assessment of Abeta and cognition in aging and Alzheimer disease. Ann Neurol 69:181–192
13. Dickson TC, Vickers JC (2001) The morphological phenotype of beta-amyloid plaques and associated neuritic changes in Alzheimer's disease. Neuroscience 105:99–107
14. Okamura N, Suemoto T, Shimadzu H et al (2004) Styrylbenzoxazole derivatives for *in vivo* imaging of amyloid plaques in the brain. J Neurosci 24:2535–2541
15. Kudo Y, Okamura N, Furumoto S et al (2007) 2-(2-[2-Dimethylaminothiazol-5-yl]ethenyl)-6- (2-[fluoro]ethoxy)benzoxazole: a novel PET agent for *in vivo* detection of dense amyloid plaques in Alzheimer's disease patients. J Nucl Med 48:553–561
16. Barthel H, Luthardt J, Becker G et al (2011) Individualized quantification of brain beta-amyloid burden: results of a proof of mechanism phase 0 florbetaben PET trial in patients with Alzheimer's disease and healthy controls. Eur J Nucl Med Mol Imaging 38:1702–1714
17. Waragai M, Okamura N, Furukawa K et al (2009) Comparison study of amyloid PET and voxel-based morphometry analysis in mild cognitive impairment and Alzheimer's disease. J Neurol Sci 285:100–108
18. Kudo Y, Furumoto S, Okamura N (2010) Benzoxazole derivatives. US Patent Application 2010/0021385
19. Shao H, Okamura N, Sugi K et al (2010) Voxel-based analysis of amyloid positron emission tomography probe [^{11}C]BF-227 uptake in mild cognitive impairment and Alzheimer's disease. Dement Geriatr Cogn Disord 30:101–111
20. McKhann G, Drachman D, Folstein M, Katzman R, Price D, Stadlan EM (1984) Clinical diagnosis of Alzheimer's disease: report of the NINCDS-ADRDA Work Group under the auspices of Department of Health and Human Services Task Force on Alzheimer's Disease. Neurology 34:939–944
21. Petersen RC, Smith GE, Waring SC, Ivnik RJ, Tangalos EG, Kokmen E (1999) Mild cognitive impairment: clinical characterization and outcome. Arch Neurol 56:303–308
22. Okamura N, Shiga Y, Furumoto S et al (2009) *In vivo* detection of prion amyloid plaques using [^{11}C]BF-227 PET. Eur J Nucl Med Mol Imaging 37:934–941
23. Kikuchi A, Takeda A, Okamura N et al (2010) *In vivo* visualization of alpha-synuclein deposition by carbon-11-labelled 2-[2-(2-dimethylaminothiazol-5-yl)ethenyl]-6-[2-(fluoro)ethoxy]benzoxazole positron emission tomography in multiple system atrophy. Brain J Neurol 133:1772–1778
24. Gauthier S, Reisberg B, Zaudig M et al (2006) Mild cognitive impairment. Lancet 367:1262–1270
25. Haroutunian V, Perl DP, Purohit DP et al (1998) Regional distribution of neuritic plaques in the nondemented elderly and subjects with very mild Alzheimer disease. Arch Neurol 55:1185–1191
26. Fodero-Tavoletti MT, Mulligan RS, Okamura N et al (2009) *In vitro* characterisation of BF227 binding to alpha-synuclein/Lewy bodies. Eur J Pharmacol 617:54–58
27. Fodero-Tavoletti MT, Smith DP, McLean CA et al (2007) *In vitro* characterization of Pittsburgh compound-B binding to Lewy bodies. J Neurosci Off J Soc Neurosci 27:10365–10371

Journals of Gerontology: BIOLOGICAL SCIENCES
Cite journal as: J Gerontol A Biol Sci Med Sci
doi:10.1093/gerona/glt041

Royal Jelly Prevents the Progression of Sarcopenia in Aged Mice In Vivo and In Vitro

Kaijun Niu,[1,2] Hui Guo,[3] Yinting Guo,[4] Satoru Ebihara,[5] Masanori Asada,[6] Takashi Ohrui,[7] Katsutoshi Furukawa,[6] Masakazu Ichinose,[8] Kazuhiko Yanai,[9] Yukitsuka Kudo,[10] Hiroyuki Arai,[6] Tatsuma Okazaki,[8] and Ryoichi Nagatomi[2]

[1]Lab of Nutritional Epidemiology, Department of Nutrition and Food Science, School of Public Health, Tianjin Medical University, Tianjin, People's Republic of China.
[2]Division of Biomedical Engineering for Health & Welfare, Tohoku University Graduate School of Biomedical Engineering, Sendai, Japan.
[3]Tianjin University of Sport, Tianjin, China.
[4]Department of Behavioral Medicine, Tohoku University Graduate School of Medicine, Sendai, Japan.
[5]Department of Internal Medicine and Rehabilitation Science, Tohoku University Graduate School of Medicine, Sendai, Japan.
[6]Department of Geriatrics and Gerontology, Division of Brain Sciences, Institute of Development, Aging and Cancer, Tohoku University, Sendai, Japan.
[7]Division of Geriatric Pharmacotherapy, Institute of Development, Aging and Cancer, Tohoku University, Sendai, Japan.
[8]Department of Respiratory Medicine, Tohoku University Hospital, Sendai, Japan.
[9]Department of Pharmacology, Graduate School of Medicine, Tohoku University, Sendai, Japan.
[10]Clinical Research, Innovation and Education Center, Tohoku University Hospital, Sendai, Japan.

Address correspondence to Kaijun Niu, MD, Lab of Nutritional Epidemiology, Department of Nutrition and Food Science, School of Public Health, Tianjin Medical University, 22 Qixiangtai Road, Heping District, 300070 Tianjin, People's Republic of China. Email: nkj0809@gmail.com

Sarcopenia is characterized by the age-related loss of muscle mass and strength. One of the mechanisms of sarcopenia is the loss in the function and number of muscle satellite cells. Royal jelly (RJ) is a health food used worldwide. To obtain better digestion and absorption than RJ, protease-treated RJ (pRJ) has been developed. RJ and pRJ have been suggested to have potential pharmacological benefits such as prolonging the life span and reducing fatigue. Because these effects may improve sarcopenia and the functions of satellite cells, we examined the effects of RJ or pRJ treatment on the skeletal muscles in an animal model using aged mice. In vivo, RJ/pRJ treatment attenuated the decrease in the muscle weight and grip strength and increased the regenerating capacity of injured muscles and the serum insulin-like growth factor-1 levels compared with controls. In vitro, using isolated satellite cells from aged mice, pRJ treatment increased the cell proliferation rate, promoted cell differentiation, and activated Akt intracellular signaling pathway compared with controls. These findings suggest that RJ/pRJ treatment had a beneficial effect on age-related sarcopenia.

Key Words: Aged mice—Sarcopenia—Satellite cells—Royal jelly—Insulin-like growth factor-1—Akt signaling.

Received September 3, 2012; Accepted March 1, 2013

Decision Editor: Rafael de Cabo, PhD

THE population of people aged 60 and older is currently growing at the rate of 2.6% per year, which is more than twice the rate of growth of the total population in the world (1). In general, aging is accompanied by frailty, functional limitations, and disabilities that interfere with the activities of daily life. These factors reduce the quality of life of the elderly patients and eventually cause their loss of autonomy in daily life. Sarcopenia is the age-related loss of the muscle mass and strength, which causes frailty, functional limitations in daily living, disabilities, and, finally, a higher mortality rate in the elderly patients (2).

Satellite cells are resident myogenic progenitors in the skeletal muscles. They play a central role in the growth and regeneration of the skeletal muscles (3). In response to stimulation, satellite cells form myoblasts, fuse together, and generate new fibers (4). The age-related functional disability and decrease in the number of satellite cells contribute to the development of sarcopenia (5). Thus, maintaining the functions of satellite cells and their numbers may reduce sarcopenia and, furthermore, may improve the regenerating capacity of the skeletal muscles in the elderly patients. However, to isolate satellite cells, specific cell surface markers were not available until recently (6).

Among the factors that stimulate satellite cells, insulin-like growth factor-1 (IGF-1) plays a central role. IGF-1 stimulates satellite cell proliferation, their differentiation into myoblasts, and, finally, their differentiation into myotubes (4). IGF-1 is the most important mediator of muscle growth and repair (7). Furthermore, a recent study suggested the potential of IGF-1 to improve sarcopenia in the elderly patients (7).

Worker honeybees produce royal jelly (RJ) in their hypopharyngeal and mandibular glands (8). RJ has been used worldwide for many years as commercially available medical products and health foods and has been considered beneficial to health. These days, a modified RJ product, protease-treated RJ (pRJ), has been developed to improve digestion and absorption compared with regular RJ. Accumulating evidence suggests that RJ is rich in a wide variety of nutrients, including vitamins, minerals, and more than 20 amino acids (9). RJ also has numerous potential pharmacological capacities, such as prolonging the life span (in mice and nematodes) (10,11) and reducing fatigue (12), hypertension (13), and hypercholesterolemia, as well as antioxidant and anti-inflammatory effects (8,14–16).

Because these effects of RJ might have a potential to improve sarcopenia and the functions of satellite cells (17–21), we hypothesized that RJ might have a beneficial effect on the prevention of sarcopenia. Furthermore, we hypothesized that this effect might involve IGF-1. To the best of our knowledge, few studies have examined the effects of RJ on muscles in elderly patients or aged animals or the relationship between RJ and IGF-1. Thus, in this study, we examined the effects of the RJ/pRJ on muscle weight, muscle strength, satellite cell functions, the regenerating capacity of the skeletal muscles in vivo and in vitro, and the involvement of IGF-1 in an animal model using aged mice.

Methods

Culture Conditions of Satellite Cells and Cell Proliferation Assay

Sorted satellite cells from untreated, aged mice were cultured in growth medium containing high-glucose Dulbecco's modified Eagle's medium with 20% fetal bovine serum (MP Biomedicals, Morgan Irvine, CA), 2.5 ng/mL basic fibroblast growth factor (Invitrogen, Eugene, OR), 100 U/mL penicillin, and 100 μg/mL streptomycin (Sigma, St. Louis, MO). Satellite cells under eight passages were used in this study. Differentiation was induced as previously shown with some modifications in differentiation medium containing high-glucose Dulbecco's modified Eagle's medium, 5% horse serum (Sigma), penicillin, and streptomycin for several days (22). RJ and pRJ were dissolved in water, sterilized by a filter, and then added to the culture medium at the following concentrations: 100, 200, 500, or 1000 μg/mL. Some cells were serum starved for overnight and then stimulated with 10 nM insulin (Sigma), which is a potent activator of Akt, for 5 minutes. The cells were cultured for 24, 48, or 72 hours, and the number of cells was determined by water-soluble tetrazolium-8 (WST-8, DOJINDO, Tokyo, Japan) assay using a cell-counting kit (23,24).

Mice and Dietary Treatment

Male C57BL/6 mice were obtained from Clea Japan (Tokyo, Japan) and maintained under specific pathogen-free conditions with unrestricted access to food and water. Experiments were carried out in accordance with guidelines established by the Tohoku University Committee on Animal Research. At the age of 21 months, mice were divided into five groups according to the diets provided for each group and maintained for the next 3 months, with 10 mice in each group. The five groups of diets were normal diet (controls), diet mixed with 1% weight RJ (1% RJ), diet mixed with 5% weight RJ (5% RJ), diet mixed with 1% weight pRJ (1% pRJ), and diet mixed with 5% pRJ (5% pRJ). All diets were manufactured by Oriental Yeast Co., Ltd. (Chiba, Japan), stored at 4°C, and sealed in plastic bags in vacuo until use to avoid oxidation. The base diet was composed of 20% milk casein, 0.3% cystine, 39.7% starch, 13.2% a-starch, 10% sucrose, 0.0014% cellulose, 1% vitamins, 3.5% mineral mixture, 0.25% choline bitartrate, and 0.5% *tert*-butylhydroquinone. The amounts of milk casein and starch were adjusted to equalize total proteins and calories between the groups in accordance with the amounts of added RJ/pRJ. Therefore, total energy and protein levels per weight were the same in all the diet groups. However, the amino acid contents were different among the groups. Dried RJ and pRJ powder was supplied by Institute for Bee Products & Health Science (Okayama, Japan). The vitamin and mineral components of RJ and pRJ were analyzed by Japan Food Research Laboratories (Tokyo, Japan) and are shown in Table 1. The mice had unrestricted access to food and water. After 3 months of the diet treatment, the grip strength was measured. Then, 25 mice (five mice from each group) were anesthetized and sacrificed, their sera were collected, and skeletal muscle samples were isolated. The other 19 (≥ 3 mice from each group) mice were sacrificed for evaluation of the regenerating capacity of injured skeletal muscles at 5 days after the injury.

Wire Hang Test

A wire mesh grid (10 × 10 cm) was used to assess the muscle strength. The mouse was placed on the wire mesh, then the mesh was inverted, and the mouse was forced to hang on the wire using its four limbs. The longest hanging time was recorded as the duration. The previously mentioned measuring process was repeated until the mouse could not hang on the wire mesh after the inversion. The number of repeated times is shown as the number of times (25).

Muscle Injury Model

After 3 months of the diet treatment, mice were anesthetized, and cardiotoxin from *Naja mossambica mossambica* (Sigma) dissolved in 100 μL phosphate-buffered saline (PBS) (10 μM) was injected into the tibialis anterior (TA) muscle. Five days later, the mice were sacrificed; and the

Table 1. Vitamin and Mineral Composition of Royal Jelly Products (mg/100 g)

Components	Royal Jelly	Protease-Treated Royal Jelly
Minerals		
Sodium	40.2	2050
Phosphorus	662	580
Iron	3.21	2.8
Calcium	40.6	44.8
Potassium	814	766
Magnesium	90.9	74.3
Copper	1.34	0.91
Zinc	6.61	5.62
Manganese	0.22	0.17
Selenium	>0.005	0.006
Vitamins		
Thiamine	0.96	0.84
Riboflavin	2.03	1.92
Vitamin B6	1.12	0.63
α-Tocopherol	0.1	>0.1
Folic acid	0.12	0.06
Pantothenic acid	12.8	14.5
Biotin	0.0467	0.0722
Inositol	>2	41
Niacin	14.8	15.4
Choline	620	480

TA muscles were isolated, frozen in 2-methylbutane precooled in liquid nitrogen, and stored at −80°C for following histological analysis (26).

Measurements of Muscle Weight and Isolation of Satellite Cells

The satellite cells were isolated according to a previous study (6) with some modifications. The large hindlimb muscles of mice including the TA muscle, triceps surae muscle, quadriceps muscle, biceps femoris muscle, gluteus maximus muscle, and iliopsoas muscle were isolated, and the weights of the muscles were measured. Next, nonmuscle tissues were removed under a dissection microscope; the muscles were subjected to enzymatic dissociation with 0.2% collagenase Type II (Worthington Biochemical Corporation, Lakewood, NJ) for 60 minutes and then with 0.04 U/mL dispase (Gibco BRL, Grand Island, NY) for 45 minutes. The cell suspension was filtered through a cell strainer (BD Bioscience, Franklin Lakes, NJ), incubated with antimouse CD16/CD32 monoclonal antibody (mAb, 2.4G2, BD Bioscience) to block Fc receptors and then with the following antibodies: fluorescein isothiocyanate–labeled anti-CD31, anti-CD45 (BD Bioscience), anti-CD11b, and anti-Sca-1 antibodies (eBioscience, San Diego, CA); PE-labeled anti-integrin-α7 (MBL, Nagoya, Japan); and Alexa 647-labeled anti-CD34 (BD Bioscience). The cells were counted and sorted by FACSAria II flow cytometer (BD Bioscience) as previously shown (27).

Immunohistochemistry and Immunocytochemistry

Frozen muscle tissues were sectioned from a region approximately 3 mm from the top of the TA muscle (8 μm in thickness) using a cryostat. For embryonic myosin heavy chain (eMyHC) staining, frozen sections or cultured cells were fixed with acetone/methanol (50%/50%) for 30 seconds at −20°C. Specimens were blocked with 1% bovine serum albumin and 0.1% Triton X-100 in PBS at room temperature for 45 minutes and then incubated with anti-eMyHC antibody (F1.652, DSHB, Iowa City, IA) at 1:2 dilution at 4°C overnight, followed by Rodamine-conjugated secondary antibody staining (Chemicon International, Temecula, CA) at room temperature in the dark for 1 hour. For PAX7 staining, cultured cells were fixed with PBS containing 4% paraformaldehyde at room temperature for 20 minutes and then blocked with 1% bovine serum albumin and 0.1% Triton X-100 in PBS at room temperature for 45 minutes. After blocking, the cells were incubated with anti-Pax-7 antibody (R&D Systems, Minneapolis, NE) at 1:50 dilution at 4°C overnight followed by Alexa 488–coupled antimouse IgG antibody (Invitrogen) at 1:200 dilution at room temperature for 1 hour. Finally, the sections or cells were mounted in Vectashield Mounting Medium with 4′,6-diamidino-2-phenylindole (DAPI) (Vector labs, Burlingame, CA). In vivo, the regenerating capacity of the injured skeletal muscles was evaluated by quantifying the percentage of eMyHc-immunoreactive area per field (28). Ten randomly selected fields at ×200 magnification were measured in each sample. ImageJ software was used to quantify the eMyHC-immunoreactive areas per field. In vitro, the degree of differentiation of satellite cells of the aged mice was evaluated by the maximum diameter of the cells by Adobe Photoshop CS2 software (San Jose, CA). The muscle sections were stained for hematoxylin and eosin also. Images were taken using a phase-contrast and fluorescence microscope BZ9000 (Keyence, Osaka, Japan) (29).

Western Blot Analysis

PAX7, Type I IGF receptor (IGF-IR), Akt, and phosphorylated Akt (phospho-Akt) proteins were detected by Western blot analysis. In brief, the cells were rinsed twice with ice-cold PBS and lysed using RIPA Lysis Buffer (Upstate, Temecula, CA). The extracted protein fraction was electrophoresed in a sodium dodecyl sulfate and 10% polyacrylamide gel and then transferred onto an Immobilon transfer membrane (Millipore, Bedford, MA). The amount of protein loaded onto the gels was 36 μg per well. The membranes were immunoblotted with the primary antibodies to PAX7 (DSHB) at 1:100 dilution, GAPDH, IGF-IR, Akt, and phospho-Akt (Cell Signaling, Boston, MA) at 1:1000 dilution. Then, the membranes were incubated with horseradish peroxidase–conjugated antirabbit immunoglobulin G (Cell Signaling) at 1:25,000 dilution, and the protein bands were detected with an

enhanced chemiluminescence detection kit (Amersham, Buckinghamshire, UK) (30).

Enzyme-Linked Immunosorbent Assay

After RJ/pRJ treatment, the mice were anesthetized with diethyl ether, and blood samples were isolated from the inferior vena cava. The serum levels of interleukin-1α (IL-1α), IL-1β, IL-6, tumor necrosis factor-α, and IGF-1 were measured using a specific ELISA kit (R&D Systems) according to the manufacturer's instructions, respectively (22).

Statistical Analysis

Data are presented as mean ± standard deviation. Differences were analyzed by one-way analysis of variance test (Post hoc, Tukey). A level of $p < 0.05$ was accepted as statistically significant. All in vitro experiments were repeated at least three times.

Results

Isolation and Characterization of Satellite Cells

As an initial step, we tried to identify the effect of RJ/pRJ on satellite cells. The characterization of satellite cells by cell surface markers has been established only very recently (6). Therefore, according to that study, we first tried to isolate satellite cells with some modifications. We enzymatically dissociated mononuclear cells from the mouse hind-limb muscles (Figure 1A, circle: upper muscles were isolated from a right leg, and lower muscles were isolated from a left leg, from left to right, TA, triceps surae, quadriceps, divided biceps femoris into two, gluteus maximus, and

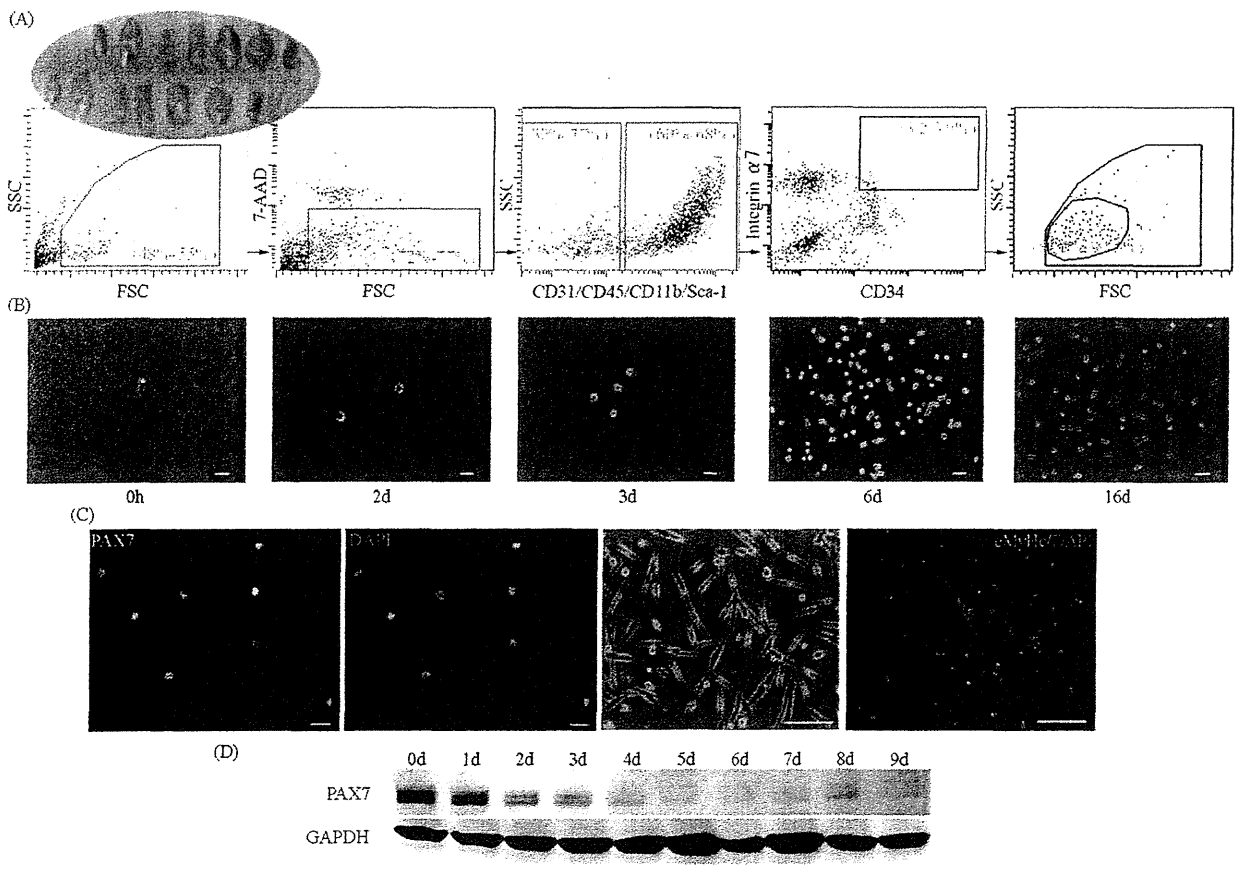

Figure 1. The isolation and characterization of the satellite cells. (**A**) A flow cytometer sorted the satellite cells from the hind-limb muscles after enzymatic dissociation (shown in circle on the left: upper muscles were isolated from a right leg and lower muscles were isolated from a left leg; from left to right: tibialis anterior, triceps surae, quadriceps, divided biceps femoris into two, gluteus maximus, and iliopsoas muscles) by gating for 7-AAD negative, then for CD31, CD45, CD11b, and Scal negative, and finally for integrin-α7 and CD34 positive. Numbers in the gates show percentage of the cells in each gate among total cells. (**B**) The light phase-contrast microscopy shows the morphology of the isolated satellite cells cultured in proliferation medium for the indicated time periods. Scale bars: 50 μm (left three panels) and 25 μm (right two panels). (**C**) The sorted cells were immunoreactive with satellite cell marker Pax7 and nucleus marker DAPI after 2 days in the proliferation medium (left two panels: Pax7 in green and DAPI in blue). After 3 days in the differentiation medium, some cells formed tube-like shapes (the third panel from the left) and some cells were immunoreactive with an immature myotube marker eMyHc (right panel: eMyHc in red and DAPI in blue). Scale bars: 20 μm (left two panels) and 50 μm (right two panels). (**D**) Western blot analysis shows the levels of PAX7 protein in the satellite cells after the induction of differentiation for the indicated time periods. The GAPDH protein is a loading control.

iliopsoas muscle) and sorted them according to the cell surface markers (Figure 1A). We characterized satellite cells as 7-AAD (a dead cell marker) negative, CD31 (an endothelial cell marker) negative, CD45 (a pan-hematopoietic cell marker) negative, CD11b (a myeloid cell marker) negative, Sca1 (a mesenchymal cell marker) negative, and integrin-α7 and CD34 positive (Figure 1A). We cultured the sorted cells in growth medium for several days and noted the proliferation of these cells, which suggested that these cells had the potential to re-enter the cell cycle (Figure 1B). After 2 days in the growth medium, the sorted cells were immunoreactive with satellite cell–specific transcriptional factor Pax7 and nucleus marker DAPI (Figure 1C, two panels in the left). To examine the potential of these cells to differentiate into myotubes, we cultured the cells in differentiation medium for 3 days (Figure 1C, two panels in the right). The cells fused and were immunoreactive with an immature myotube marker embryonic myosin heavy chain (eMyHc, Figure 1C, the right panel), suggesting that the cells differentiated into myotubes. The sorted cells were cultured in the differentiation medium, and the expression levels of Pax7 gradually decreased in a time-dependent manner after the induction of differentiation (Figure 1D). These data suggested that the sorted cells had the characteristics of satellite cells and the potential to differentiate into myotubes.

Effects of RJ/pRJ on the Satellite Cells of the Aged Mice In Vitro

To examine the effect of RJ/pRJ on the proliferation rate of the satellite cells of the aged mice in vitro, we isolated satellite cells from aged mice and stimulated them with RJ/pRJ for 24 hours (Figure 2A, left panel), 48 hours (Figure 2A, center panel), or 72 hours (Figure 2A, right

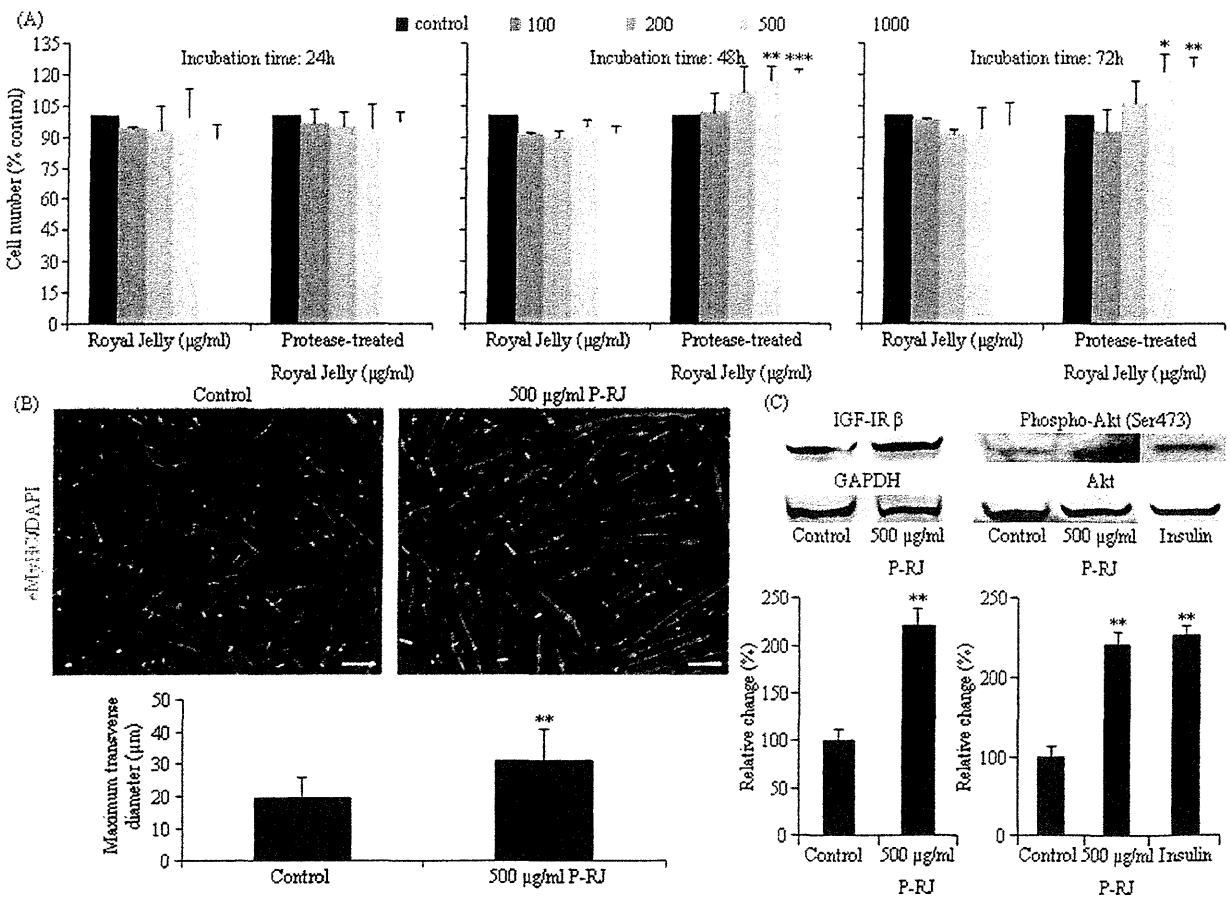

Figure 2. Effects of RJ/pRJ on the satellite cells of aged mice in vitro. (**A**) The satellite cells of the aged mice were treated with the indicated concentrations of RJ or pRJ for 24, 48, or 72 h, and the cell proliferation rate was measured at each time point. (**B**) The satellite cells of aged mice were cultured in differentiation medium with pRJ or without pRJ (control) for 5 days, then immunohistochemically stained for eMyHC in red and for DAPI in blue to evaluate their differentiation into myotubes. The maximum diameter of each myotube was marked with a green line (upper panels). We randomly selected 50 myotubes per field at ×400 magnification, measured the maximum diameter of each myotube for 10 randomly selected fields per sample, measured the diameter, and calculated for each group (lower panel). Scale bars: 100 μm. (**C**) The satellite cells of aged mice were pretreated with pRJ (500 μg/mL) for 48 h, then the Western blot analysis detected IGF-1 receptor (IGF-IR), GAPDH, activated form of Akt (phospho-Akt), and total Akt. Insulin (10 nM) was used as a positive control. The densitometry quantified the band intensities. The graphs show the IGF-IR band intensities normalized by the GAPDH band intensities, and phospho-Akt band intensities normalized by the Akt band intensities. This figure is the representative of three independent experiments. Columns are mean ± *SD*. $^{*}p < .05$, $^{**}p < .01$, and $^{***}p < .0001$, compared with control.

panel) in growth medium. pRJ treatment at high concentrations (500 and 1000 μg/mL) for 48 and 72 hours increased the proliferation rate of the satellite cells compared with controls and RJ treatment (Figure 2A). Next, to examine the effect of RJ/pRJ on the differentiation of the satellite cells of the aged mice in vitro, we cultured the satellite cells in differentiation medium for 5 days and immunohistochemically stained them for eMyHC (Figure 2B). The pRJ-treated group had more eMyHc immunoreactive areas than did the controls (Figure 2B, upper panel). The mean maximum diameter of the myotubes was greater in the pRJ-treated group than in the controls (Figure 2, lower panel). These results suggested that pRJ promoted the differentiation of the satellite cells of the aged mice. We next examined an intracellular signaling pathway of IGF-1 by Western blot analysis. pRJ treatment increased the intensity of the band of IGF-1R compared with controls (Figure 2C). One of the downstream signaling pathways of IGF-1R is Akt, and pRJ treatment increased the intensity of the band of phosphorylated Akt, which is an activated form of Akt, compared with controls (Figure 2C). Similar to pRJ, the increased activation of Akt was also observed in satellite cells treated with 10 nM insulin (Figure 2C). These results suggested that pRJ increased the proliferation rate, promoted differentiation, and activated the Akt-signaling pathway in the satellite cells from the aged mice compared with the controls in vitro.

RJ-/pRJ-Treated Mice Had Greater Numbers of Satellite Cells, Muscle Weight, and Grip Strength Than Did Controls

To examine the effects of RJ/pRJ treatment on aged mice in vivo, we divided 21-month-old mice into five groups and treated them with five kinds of diets for 3 months, respectively: normal diet (controls), diet mixed with 1% weight RJ (1% RJ), diet with 5% weight RJ (5% RJ), diet with 1% weight pRJ (1% pRJ), and diet with 5% pRJ (5% pRJ). Three mice in the controls, one mouse in the 1% RJ group, and one mouse in the 1% pRJ group died of natural causes during the treatment period. These mice were excluded from the analysis. During the intervention period, the body weight increased similarly in RJ/pRJ-treated groups and control groups (Figure 3A) (p value > .73; effect size ≤ 0.01). The amount of daily diet intake was not different between the groups (Figure 3B). Comparison of the hind-limb muscle weight per body weight between 2-, 8-, and 24-month-old mice showed progressive loss of muscle weight with aging, suggesting the progression of sarcopenia with aging (Figure 3C). The combined weights of the hind-limb muscles of one leg, named one-legged muscle, per body weight in 5% RJ, 1% pRJ, and 5% pRJ groups were greater than those of controls (Figure 3D). The selected muscles included the TA, triceps surae, quadriceps, biceps femoris, gluteus maximus, and iliopsoas muscles. To examine the effect of PJ/pRJ on the numbers of satellite cells in vivo, we counted the cells. The numbers of satellite cells in the hind-limb muscles in the 5% RJ- and 5% pRJ-treated groups were significantly greater than those of the controls (Figure 3E), whereas the numbers of the satellite cells per muscle weight were not different among the groups (per gram; Figure 3F). These results suggested that PJ/pRJ treatment increased the total numbers of satellite cells.

To examine the effect of pRJ on the muscle strength, we performed the wire hang test and measured the maximum duration that the mice could hang on the inverted wire mesh. Consistent with the effect of RJ/pRJ on the muscle mass, the 5% RJ- and 5% pRJ-treated groups hung for longer duration than did the controls, suggesting that RJ/pRJ improved the grip strength of the skeletal muscles (Figure 3G). To examine the effect of RJ/pRJ on muscle fatigue, we measured how many times the mice could hang from the wire mesh. The 5% RJ- and 5% pRJ-treated groups could hang more times than the controls, suggesting that RJ/pRJ improved the fatigue of the skeletal muscles (Figure 3H). Furthermore, within the controls, comparison of the before and after treatment period showed decreased hanging duration and times after the treatment period than before, suggesting the progression of age-related atrophy in muscle function. In contrast, no significant changes were observed within the RJ/pRJ groups between before and after the treatment period. These data suggested that RJ/pRJ treatment prevented the progression of atrophy in muscle weight and function in the aged mice.

RJ/pRJ Treatment Accelerated the Regeneration of Injured Skeletal Muscles

We next examined the effect of RJ/pRJ treatment on the regenerating capacity of the skeletal muscles in aged mice in vivo by injuring the TA muscles with cardiotoxin injection and observing their regeneration. We isolated the muscles 5 days after the cardiotoxin injection and subjected them to staining. Hematoxylin and eosin staining showed greater amounts of muscle fibers in the RJ/pRJ groups than in the controls (Figure 4A, upper panels). To confirm the regenerating capacity of the skeletal muscles, we immunohistochemically stained the muscles for eMyHc, which is a marker of immature myotubes including regenerating muscles but not of mature muscles (Figure 4A, middle line panels). Quantification of the eMyHc immunoreactive area showed greater immunoreactive areas in the RJ/pRJ groups than in the controls (Figure 4B). These results suggested that RJ/pRJ treatment accelerated the regeneration of the injured skeletal muscles.

RJ/pRJ Treatment Increased Serum IGF-1 Levels

Because RJ has been suggested to have an anti-inflammatory effect, we examined the effect of RJ/pRJ treatment on serum proinflammatory mediator levels in the aged mice.